Colloid Polym Sci (2008) 286:1317–1327
DOI 10.1007/s00396-008-1903-1

ORIGINAL CONTRIBUTION

"Sweet" gold nanoparticles with oligosaccharide-modified poly(ethyleneimine)

Anja Köth · Joachim Koetz · Dietmar Appelhans · Brigitte Voit

Received: 20 February 2008 / Revised: 26 May 2008 / Accepted: 12 June 2008 / Published online: 15 July 2008

Abstract This paper is focused on the use of oligosaccharide-modified hyperbranched poly(ethyleneimines) (PEI) as reducing and stabilizing agent for the formation of gold nanoparticles. The results show that the secondary amino groups of the PEI as linear units are responsible for the reduction process, and the primary amino groups as terminal units are of relevance for the particle stabilization. With regard to the final size and shape of the gold nanoparticles formed, the amount and type (maltose or maltotriose) of oligosaccharide units and structural parameters of the PEI samples are of importance. The smallest particle size of about 2 nm is obtained from a maltose-modified PEI with an excess of linear units. The size and shape of the polymer-stabilized nanoparticles can be further tuned by changing the solute concentration, the time of heating, as well as the pH value.

Keywords Oligosaccharide-modified poly(ethyleneimine) · Gold nanoparticles

Introduction

The process for making colloidal gold has been known already for a long time period. Recently, the preparation of colloidal gold has received a reincarnation due to its special, size-related electronic, conductometric, magnetic, and optical properties [1–3].

Ultrafine gold nanoparticles have attained considerable attention since they can offer highly promising and novel options for a wide range of applications, e.g. in catalysis and optical sensing. Gold nanoparticles are used as electron-dense labelling agents in histochemistry and cytochemistry, and they also improve the catalytic activity of palladium and platinum catalysts [4]. Recent years have seen tremendous progress in the field of biology and biomedicine, and gold nanoparticles have been successfully used for example in cancer diagnostics and therapeutics [1], as well as in immunoassays [5–7].

Caused by the high activity towards oxygen, gold nanoparticles offer new possibilities in oxidative catalysis [8–9]. Furthermore, colloidal gold particles have been used in pollution and automobile exhaust emission control processes [10].

Several procedures are already well-established for the synthesis of gold nanoparticles from a diluted tetrachloroaureate solution. Different components, e.g. tannin, urine, citric acid, oxalic acid or borhydride, can be employed as reducing agents [1, 4, 11]. In the case of charged reducing agents, e.g. citric acid or oxalic acid, an electrostatically stabilized colloidal system is formed. Turkevich et al. [11] have investigated the reduction process with citric acid in more details already 50 years ago. They were able to show that the synthesis can be subdivided into a nucleation and growth process. The primary formed nuclei with diameter of about 3 nm then start to grow. Finally 15–17-nm-sized gold particles are formed. Recently published EM micrographs and dynamic light scattering data confirm these results very well [12].

Another possibility to stabilize especially very small gold nanoparticles, or so called gold clusters, is to use phosphine [13] or alkanethiolate ligands [14].

A. Köth · J. Koetz (✉)
Institut für Chemie, Universität Potsdam,
Karl-Liebknecht-Strasse 24–25, Haus 25,
14476 Potsdam (Golm), Germany
e-mail: koetz@rz.uni-potsdam.de

D. Appelhans · B. Voit
Leibniz-Institut für Polymerforschung Dresden e.V.,
Hohe Strasse 6,
01069 Dresden, Germany

If the colloids are noncharged, they tend to aggregate. Therefore, an additionally stabilizing agent is required. To overcome this problem protecting components have to be added, which can adsorb at the particle surface and prevent the agglomeration due to a steric stabilization. Especially, poly(vinylpyrrolidone), poly(ethylene glycol) and their copolymers [15–17] are utilized, as well as amphiphilic block copolymers [18–20]. By using polyelectrolytes the steric stabilizing effect combined with the electrostatic one lead to the electrosteric stabilization. Therefore, polyelectrolytes are of special interest for stabilizing colloidal dispersions, in particular gold nanoparticles [12, 21–24].

It was recently shown that linear and branched poly (ethyleneimines) produce gold nanoparticles in aqueous solutions in the absence of further reducing agents [25–31]. In the first step the poly(ethyleneimines) (PEI) reduce the gold ions and then the gold nanoparticles are formed finally surrounded by the PEI. Chen et al. checked the effects of poly(ethyleneimines) with alkyl side chains on the formation of gold colloids. They were able to show that the hydrophobicity of the polyelectrolyte influences the particle morphology. The hydrophobic side chains induce the formation of polymer micelles, which seem to be responsible for the formation of nanoparticles with different shapes, e.g. triangles and hexagons [25]. Saccharide-modified hyperbranched PEI and poly(amidoamines) (PAMAM) are already applied for producing Au nanoparticles, but only under the use of $NaBH_4$ [32]. PAMAM glycodendrimers demonstrated reductive properties, but a detailed discussion of the mechanism of the reduction process is missing in the literature [33]. It has to be stated here that other approaches to synthesize gold glyconanoparticles from free oligosaccharides or RAFT synthesized glycopolymers are already well-established [33–36].

Taken this knowledge into account the goal of our research activities is to produce and stabilize Au nanoparticles of very small dimensions, stabilized by weak polyelectrolytes. Due to the interesting optical properties of well-defined colloidal gold nanoparticles, they are of special interest in cancer diagnostic and therapy [2] and gold nanoparticle-based immunoassays [5]. For biomedical purposes, high biocompatibility and noncytotoxicity have priority under buffer solution conditions required for biological studies without the need for previous dialysis steps. For example poly(ethylene glycol)-coated colloidal gold nanoparticles show a biocompatibility without cytotoxicity in the mouse [37]. Oligosaccharide-modified hyperbranched poly(ethyleneimines) seem to fulfil the requirements of biocompatibility and noncytotoxicity.

In the present work the reduction and stabilization process to colloidal gold is made by adding different well-defined oligosaccharide-modified poly(ethyleneimines) to a highly diluted gold chloride solution at room temperature and 100 °C, respectively. The aim of the research is to understand the role of the oligosaccharide architectures on the mechanism of the reduction and stabilization process with regard to the degree of oligosaccharide substitution and type of oligosaccharide unit.

Experimental

Materials

The oligosaccharide-modified hyperbranched poly(ethyleneimine) samples I–VII (schematically demonstrated in Fig. 1) were synthesized via a reductive amination of the hyperbranched PEI, with M_w of 5,000 and 25,000 g/mol, respectively, with maltose or maltotriose in sodium borate solution under similar conditions already described in Ref. [38, 39]. In order to achieve the structure A–C, shown in Fig. 1, the molar ratio of PEI and oligosaccharide was 1:5 for structure A, 1:0.5 for structure B, and 1:0.2 for structure C. Further details of the synthesis and characterization of the maltose- and maltotriose-modified PEI will be published soon.

The metal precursor hydrogen tetrachloroaureate $HAuCl_4$ was purchased from Aldrich. Water was purified with the Modulab PureOne water purification system (Continental).

Colloidal gold preparation

Aqueous solutions of the various oligosaccharide-modified PEI (1% by weight) were prepared and stirred 24 h before use. Aqueous tetrachloroaureate solution (2 mM) was freshly prepared.

In procedure A each polyelectrolyte solution was mixed with the metal precursor solution in a weight ratio of polyelectrolyte and metal=1:1 (molar ratio, ca. 1:0.75) at room temperature.

In procedure B each polyelectrolyte solution was mixed with the metal precursor solution in a weight ratio of polyelectrolyte and metal=1:1 (molar ratio, ca. 1:0.75), and heated up for 30 min to 100 °C

In procedure C each polyelectrolyte solution was mixed with the metal precursor solution in a weight ratio of polyelectrolyte and metal=1:10 (molar ratio, ca. 1:7.5), and heated up for 3 min to 100 °C.

The pH-dependent measurements were made according to procedure A at room temperature.

Methods

To characterize the particle size and size distribution, dynamic light scattering (DLS) measurements were carried

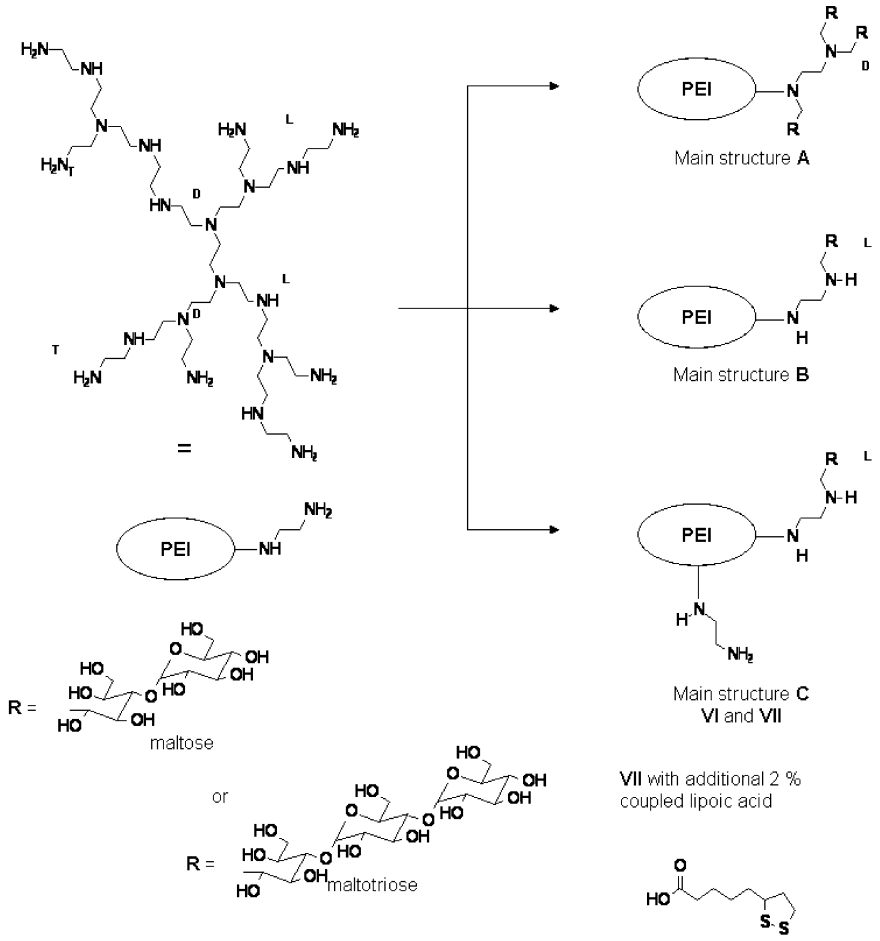

Fig. 1 Chemical structures of the different PEI samples

Sample	Structure	OS[a]	T unit[a,b]	L unit[a,b]	D unit[a,b]	PEI – M_w[c]
			%	%	%	*g/mol*
I	A	maltose	-	9.4	90.6	5000
II	A	maltose	-	14.4	85.6	25000
III	B	maltose	-	65	35	5000
IV	B	maltotriose	-	38	62	25000
V	C	maltotriose	10	34	56	5000
VI	C	maltotriose	16	53	31	5000
VII	C	maltotriose	14	52	34	5000

[a] OS = oligosaccharide; T = terminal, L = linear, D = dendritic; determined by elemental analysis. [b] As one example for unmodified PEI with 5000 g/mol: 32 % T units, 36.7 % L units and 30.7 % D units. [c] Unmodified PEI with M_w 5000 or 25000 g/mol was converted with maltose or maltotriose.

out at 25 °C at a fixed angle of 173° using the Nano Zetasizer (Malvern), equipped with a He–Ne laser (4 mW) and a digital autocorrelator. It has to be mentioned here that this 173° backscatter detection technique is a useful method to detect particles of very small dimensions down to 1 nm. Recently published data show that subnanometer measurements are achievable with a precision of 0.1 nm [40].

However, the data observed have to be analyzed very carefully. Note that only measurements with a good fit and an exponential graphic representation were considered here.

The particle size distribution was determined by using a multimodal peak analysis by intensity, volume, and number, respectively. The intensity-based distribution that means the most sensitive method for larger particles or particle aggregates shows a peak splitting (two or three peaks appear) in some cases, but the number-based distribution outlines preferably one peak in the most cases. The mean particle size listed in the tables is the average value of ten measurements by using the multimodal peak analysis by number. The z-average was used as given.

The zeta potential, that means the electrokinetic potential at the effective shear plane between the moveable and nonmovable part of the double layer, was measured by means of the Nano Zetasizer (Malvern) based on the principle of electrophoretic light scattering [12].

UV-vis experiments were performed with a Cary 5000 UV-vis NIR spectrometer (Varian) in quartz cuvettes with a path length of 1 cm.

In comparison to the dynamic light scattering experiments the morphology and size of the particles were determined by transmission electron microscopy (EM 902, Zeiss). Samples were prepared by dropping the colloidal dispersion on the copper grids. After air drying the samples were examined in the transmission electron microscope at an acceleration voltage of 90 kV.

Results and discussion

First of all it has to be mentioned here that a gold chloride solution can be reduced by adding the unmodified hyperbranched PEI samples with a molar mass of M_w=5,000 g/mol and M_w=25,000 g/mol by heating up the system to 100 °C (according to procedures B and C), but not at room temperature. The z-average of the particle size, determined by means of dynamic light scattering, varies between 16 and 19 nm, and the red colored solutions exhibit an UV maximum between 522 and 524 nm. Note that similar results were observed by using a commercially available PEI product (Polymin P, BASF) [29].

In order to understand the dual function of the PEI as reducing and stabilizing agent, the structures A–C of different hyperbranched PEI I–VII are schematically presented in Fig. 1. The following structure differences are given based on the modification of hyperbranched PEI with terminal (T) (primary amino groups), linear (L) (secondary amino groups) and dendritic (D) units (tertiary amino groups) (compare Fig. 1):

1. Structure A for I and II consists of an excess of D units since the former T units were mainly converted into D units, possessing two chemically coupled oligosaccharide units as surface groups.
2. Structure B, especially for III, mainly possesses L units since the former T units were converted into L units, having one chemically coupled oligosaccharide as surface group. IV has only of about the half of L units than III.
3. Structure C differs from structure B due to the presence of additional T units remaining as surface groups after the modification step.

The oligosaccharide-modified PEI samples I–VII, varying in the degree of substitution and the molar mass, were used as a reducing and stabilizing agent for the formation of gold nanoparticles. First of all our experiments show no color effect in presence of the samples I and II. Already Wang et al. [41] speculated that predominantly the secondary amino groups are responsible for the reduction process. In full agreement to this, our experimental findings demonstrate that the dominant tertiary amino groups in I and II are unable to reduce a gold chloride solution. Therefore, one can conclude that only the secondary and/or primary amino groups have a reducing power.

Gold nanoparticle formation at room temperature (procedure A)

After mixing the oligosaccharide-modified PEI solution (1 wt.%) with the $HAuCl_4$ solution in a mass ratio of 1:1 (molar ratio, ca. 1:0.75), the mixtures were stirred at room temperature and the color effect after 5 days was noted (procedure A). Thus, the mixtures in presence of samples I and II remain colorless, and only with samples III–VII a color effect with time is observed. In presence of sample V the solution becomes red, and with samples III, IV, VI, and VII brown.

When small spherical metallic nanoparticles are irradiated by light, the oscillating electric field causes the conduction electrons to oscillate coherently. The collective oscillation of the electrons is called dipole plasmon resonance [42]. “Classical” red colored colloidal gold sols produced by the route described by Turkevich [11] with a particle size of about 20 nm show an absorption maximum at about 520 nm, which strongly depends on the particle size, the type of stabilizer, and step of aggregation [1, 12, 29]. Our own experiments with such a citrate-stabilized colloidal

gold sol, containing nanoparticles of about 17 nm in size, show a significant increase of the particle size by DLS after adding low molecular salts. Also a cluster aggregation is observed in transmission electron microscopy (TEM) micrographs combined by a color change to blue. However, this can be well-explained by an aggregation of the electrostatically stabilized nanoparticles according to the classical DLVO theory [12]. Another possibility to induce an aggregation is to add polymers [12]. For example single-stranded DNA adsorbs at negatively charged gold nanoparticles in contrast to double-stranded DNA.

Li et al. [6] presented evidence that this adsorption phenomenon can be explained by the difference in their electrostatic properties that in turn reflects conformational differences.

Mirkin et al. have already shown that S-bonded DNA oligomers can stabilize gold nanoparticles significantly [43]. The DNA-mediated reversible assembly of gold nanoparticles has been investigated in many studies [43–46], and can lead to a DNA-guided crystallization of gold nanoparticles [47].

The DNA-induced aggregation process can be utilized to design simple colorimetric and fluorimetric assays [6]. It has to be stated here that such gold nanoparticle assays mainly depend on the aggregation/immobilization of the particles.

Furthermore, subnanometer-sized gold clusters show an absorption in the 400–420 nm range. For example undecagold (Au_{11}) clusters with diameter of about 0.8 nm exhibit an absorption maximum at 415 nm, which has been suggested to the 5d → 6s interband transitions in the cluster core [13]. Note that the optical absorption and fluorescence of the clusters are very sensitive to the surface protecting ligands used. For instance, the particle band gap and luminescence is changed by substitution of triphenylphosphine ligands by alkanethiolates [14].

One of the best known methods of preparing gold clusters with subnanometer size is using sodium borohydride in the presence of triarylphosphanes.

Recently, the crystal structure, electrochemical, and optical properties of such gold nanoclusters are characterized in more detail [48, 49]. In general it has to be stated here that the ligands can induce the formation of differently sized clusters.

Our colored gold solutions show typical UV absorption bands in the region between 400 and 550 nm. The UV-vis-spectra plotted in Fig. 2 exhibit only in the case of sample V one absorption maximum at 519 nm, which can be related to the plasmon oscillation effect of colloidal gold particles with particle dimensions of about 20 nm. All other samples show a second absorption band at about 420 nm, which can be related to significant smaller gold clusters.

In the presence of sample III and IV this leads to a plateau between 420 and 520 nm. By using sample VI a main absorption is observed at 425 nm, and a shoulder at 520 nm. In the presence of sample VII the absorption band

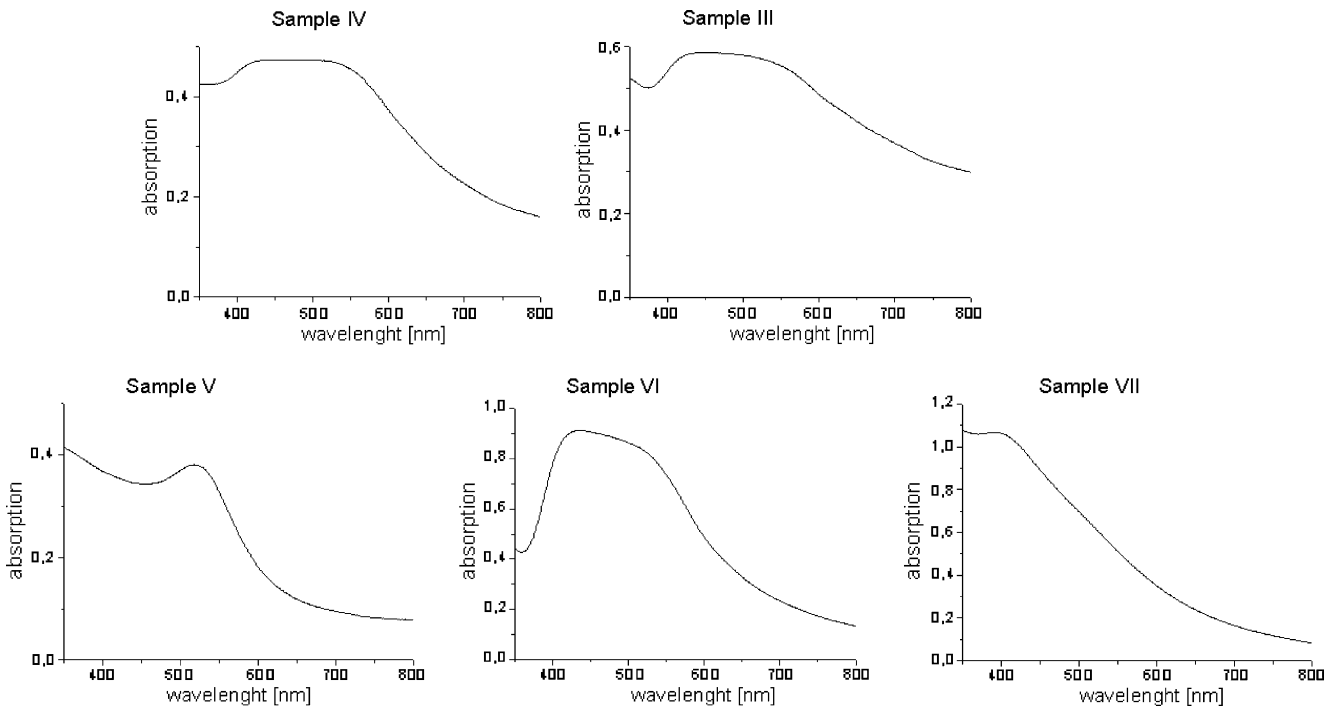

Fig. 2 UV-vis spectra of gold nanoparticles prepared at room temperature according to procedure A with samples III to VII

at 520 nm disappears, and only the absorption maximum at 410 nm can be observed, suggesting the formation of significant smaller particles.

Dynamic light scattering is a useful method to determine the particle size and particle size distribution of nanoparticles. However, it was found that the results obtained in this study depend on the analysis program (Contin, Monomodal, Multimodal, or Automatic) which evaluates the intensity, the number or the volume of particle size distribution, respectively. In our experiments we analyzed a mean particle size, that means an average value from ten repeat series, obtained from the multimodal peak analysis by number. The data, listed in Table 1, show that the mean particle size varies between 1.7 and 4.7 nm for different PEI derivatives.

To clarify that the measured data can be related primarily to the gold nanoparticles, we have evaluated in addition the scattering behavior of the PEI samples alone.

For the unmodified PEI with a M_w of 5,000 g/mol we obtained a z-average value of 4.4±0.2 nm, and for the unmodified PEI with M_w=25,000 g/mol a value of 7.2± 0.1 nm. The hydrodynamic radius of the oligosaccharide-modified PEI samples is in the same order: 5.3±0.2 nm for I, 6.8±0.2 nm for V, and 5.8±0.1 nm for VI.

On the one hand these experiments demonstrate that DLS is suitable to detect the hydrodynamic radius of the polymers. On the other hand the results clearly show that the coil dimensions of the polymer molecules are larger than the finally detected particle dimensions of the colloidal gold sols. More detailed measurements have shown that both peaks coexist in the presence of gold nanoparticles and poly(ethyleneimine). In the intensity plot, a dominant nanoparticle peak and a significant smaller polymer peak can be observed. The last one disappears in the number plot. Therefore, it is possible to detect primarily the gold nanoparticles by the number-based DLS analysis. This result is based on the much better scattering contrast of the gold particles in the solution.

On closer examination, two peaks in the intensity plot (compare Table 1) were assigned for the brown solution of sample IV with the plateau range between 420 and 520 nm, but only one in the number plot. This indicates a bimodal particle size distribution in which the small nanoparticle fraction is in excess. A splitting into two fractions in the intensity plot with a dominant small particle fraction, can be observed for all samples, given in Table 1.

Table 1 shows that the smallest mean particle dimensions of about 2 nm are observed in presence of sample III and VII (Table 1).

Significant larger particle dimensions were detected for the red colored solution with sample V where the part of the larger particle fraction, as to be seen in the intensity plot, is in excess. The mean particle size is increased and the size distribution becomes larger.

Combining the results from UV-vis spectroscopy and dynamic light scattering one can conclude that the particle fraction with particle dimensions of about 2 nm for the gold cluster fraction in the brown colored Au solution is responsible for the absorption band at ca. 420 nm. The particle fraction with diameter ≥4 nm can be related to the red color with a typical UV absorption at ca. 520 nm indicating a plasmon resonance.

Transmission Electron Microscopy is a powerful method to visualize the particle dimensions. The TEM micrographs indeed show the existence of a particle fraction with very small diameter of about 2 nm and, in addition, a second particle fraction of significant larger dimensions. Exemplary, the histogram of Fig. 3 indicate a splitting in two particle fractions of about 2 and ≥4 nm, which is in full agreement with the mean particle size obtained by dynamic light scattering (3.7±1.6 nm). However, also some larger particles exist with diameter >10 nm.

In the red colored solution with sample V the particle fraction with diameter of about 7 nm becomes dominant. Thus spherical gold nanoparticles are formed, shown in Fig. 4. Note that TEM micrographs are obtained after drying the gold sol on the EM grid. Therefore the obtained particle aggregate structures have to be discussed with care.

In summary, the results, received by UV-vis, DLS, and TEM, demonstrate that the particle fraction of very small

Table 1 Features of the samples III to VII prepared at room temperature

Sample	Color	Zeta potential [mV]	Mean particle size of DLS [nm]	Particle size fractions in the intensity plot of DLS [nm]	UV-VIS (λ_{max})
III	brown	31±2.1	1.7±0.5	1.6±0.4; 5.7±0.9	Plateau from 425 to 505 nm
IV	brown	17±1.5	3.7±1.6	3.9±1.5; 18.3±8.6	Plateau from 425 to 520 nm
V	red	12±0.8	4.7±2.8	3.6±1.4; 12.8±4.6	519 nm
VI	brown	11±2.9	3.3±1.0	3.7±1.1; 19.0±8.0	425 nm, shoulder at 520 nm
VII	brown	11±3.2	2.2±0.9	2.3±0.8; 8.8±3.4	410 nm

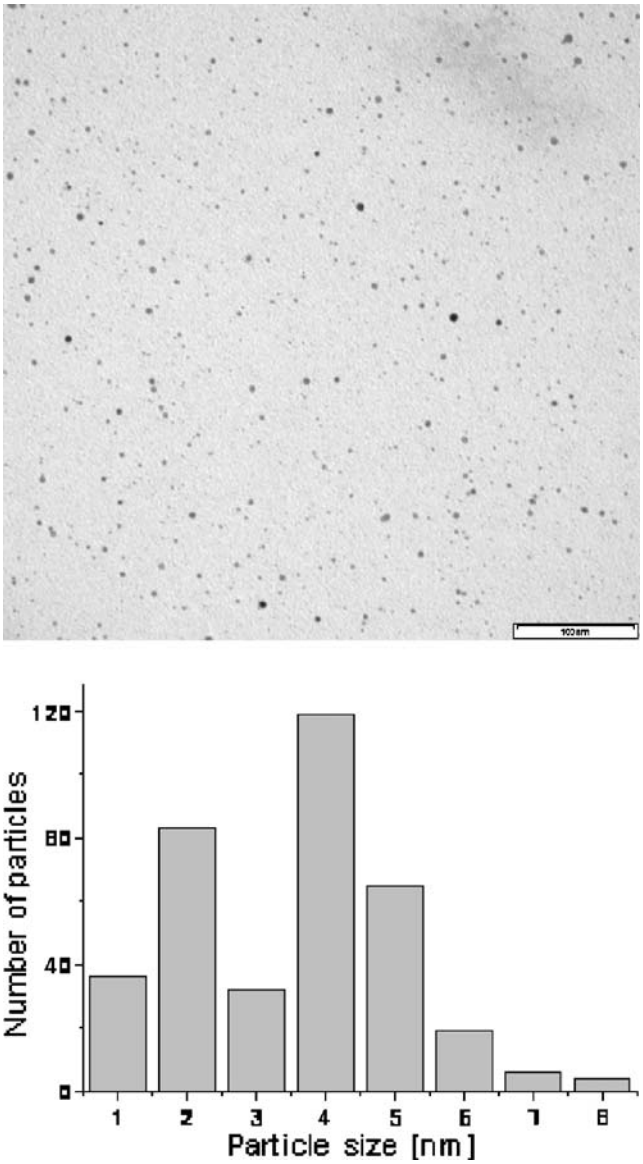

Fig. 3 TEM micrograph and histogram of gold nanoparticles prepared at room temperature according to procedure A with sample IV

dimensions (ca. 2 nm in size) is related to the UV maximum at 420 nm, and the fraction of larger colloidal gold particles with diameter of ≥4 nm can be related to the absorption band at 520 nm.

Usually, one would expect that the hydrodynamic radius (determined by DLS) must be larger than the radius measured in TEM micrographs, when the polymer is adsorbed at the particle surface. However, we do not find differences in the particle size by using DLS and TEM, that means there is no experimental hint for core-shell particles with a polymer coating layer. Taking this into account one can assume that the gold nanoparticle nucleation process starts at the secondary amino groups "inside" the polymer coil, and the particle growth leads to "collapsed" polymer molecules. To underline this explanation additional SANS measurements in water and D_2O are in progress.

The surface charge of the Au nanoparticles can be analyzed by a particle electrophoresis. Therefore, additional zeta potential measurements were performed. The positive zeta potential, detected for the modified PEI samples III–VII, varies between +11 and +31 mV (Table 1). This means the nanoparticles are electrostatically stabilized.

Furthermore, the zeta potential in presence of sample III with +31 mV is much higher than in all other cases, which can be related to the polymer structure type B with an excess of linear units (compare Fig. 1). Generally, in the presence of type C PEI samples (samples V–VII) possessing the more voluminous maltotriose units the electrostatic stabilization seems to be not so effective.

Due to the fact that the unmodified hyperbranched PEI samples with a M_w of 5,000 and 25,000 g/mol are not able to reduce a gold chloride solution at room temperature, our experiments revealed further knowledge about reduction and stabilization properties of PEI samples modified with maltose and maltotriose:

1. The structure type A (sample I and II) with predominantly dendritic units cannot be used as a reducing agent. However, in the presence of oligosaccharide-modified PEI samples with significant amounts of linear units (structure type B) or additional terminal units (structure type C) the reduction power is high enough to produce gold nanoparticles.

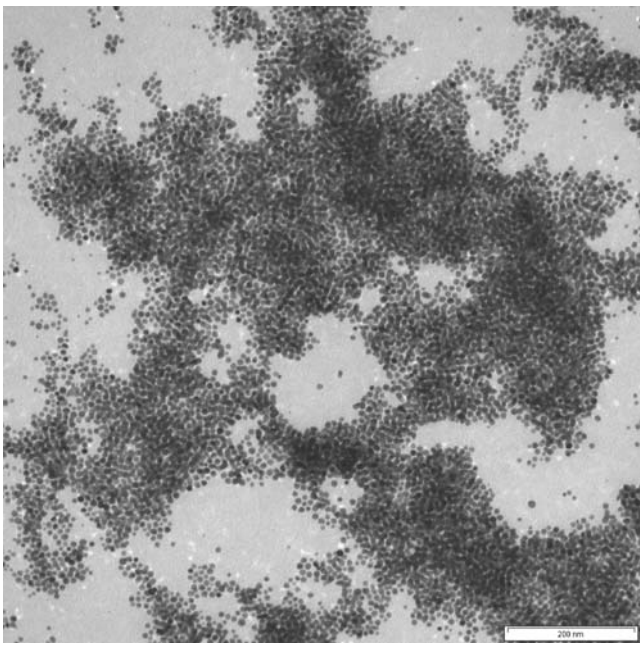

Fig. 4 TEM micrograph of gold nanoparticles prepared at room temperature according to procedure A with sample V

Fig. 5 Scheme of the reduction mechanism according to [41]

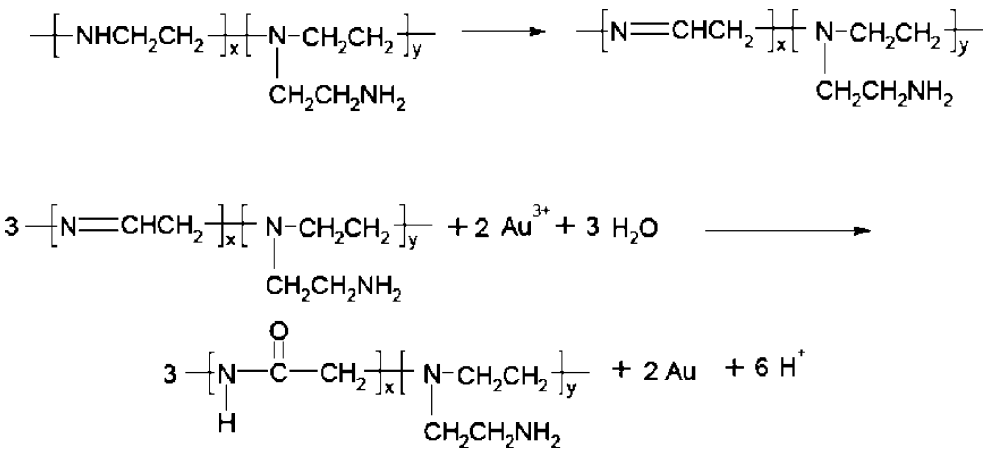

2. The incorporation of maltose or maltotriose units in the outer sphere of the PEI macromolecule leads first of all to the formation of ultra fine gold nanoparticles, or so called Au clusters, in the order of 2 nm in size. Thus, the subsequent growing process of the gold nuclei, according to the mechanism proposed by Turkevich [11], is hindered due to the additional steric stabilizing effect of the oligosaccharide surface groups, which is more pronounced in presence of the maltotriose units.
3. When structure type B is used, the electrostatic stabilization is better in the presence of linear units possessing maltose units (sample III), but the steric stabilization can be improved by using maltotriose units (sample IV). In the presence of structure type C the particle size and particle size distribution mainly depend on the ratio between the terminal, linear, and dendritic structure elements (T, L, and D ratio given in Fig. 1).
4. Larger gold particles with uniform particle size, showing the typical plasmon resonance, can be obtained with the more dendritic PEI sample V, when the number of terminal primary amino groups is fixed at a lower level of about 10%.
5. A partial amidation of the amino groups with 2% lipoic acid leads to a much better stabilization of the small particle fraction due to a better adsorption of the polymer on the gold nanoparticle surface.

Table 2 Features of the samples III to VII prepared at 100 °C (30 min; weight ratio of PEI, metal=1:1)

Sample	Color	Zeta potential [mV]	Mean particle size DLS [nm]	UV-VIS (λ_{max})
III	brown	21±1.6	1.5±0.5	Plateau from 435 to 505 nm
IV	brown	22±1.6	3.5±1.7	Plateau from 430 to 560 nm
V	red	13±0.4	8.6±3.0	519 nm
VI	brown	16±2.0	2.5±1.0	Plateau from 460 to 540 nm
VII	Brown	30±2.6	2.6±0.7	420 nm

In summary of all these facts, one conclusion is that the reducing power is related predominantly to the linear units (secondary amino groups) according to a reduction mechanism already proposed by Wang et al. [41], which is schematically presented in Fig. 5.

In the first step ion pairs between the negative chloroaurate ions and the protonated amino groups are formed, and in a second step instable double bounds are generated. Finally, the reaction leads to the formation of amide bounds.

Gold nanoparticle formation at 100 °C (procedure B, 30 min; weight ratio of PEI is to metal=1:1)

Recently, we have shown that the reducing power of the branched PEI can be enhanced by heating up the solution [29]. Therefore, the mixture of oligosaccharide-modified PEI and $HAuCl_4$ solution was heated in an oil bath up to 100 °C for 30 min. PEI samples I and II do not reduce the Au^{3+} solution, but all other samples show a color change after cooling down the mixtures to room temperature. Brown colored solutions were obtained in presence of samples III, IV, VI, and VII. A red colored Au solution was observed only in presence of sample V.

The UV-vis spectra are similar to the spectra of gold solutions obtained according to procedure A at room

Table 3 Features of the samples III, IV, VI and VII prepared at 100 °C (3 min; weight ratio of PEI, metal=1:10)

Sample	Color	Zeta potential [mV]	Mean particle size DLS [nm]	UV-VIS (λ_{max})
III	red	39±2,3	8.6±3.0	561 nm
IV	red	36±1,7	15.1±7.1	552 nm
VI	red	42±2,8	9.4±3.7	524 nm
VII	red	33±3,7	10.2±4.5	524 nm

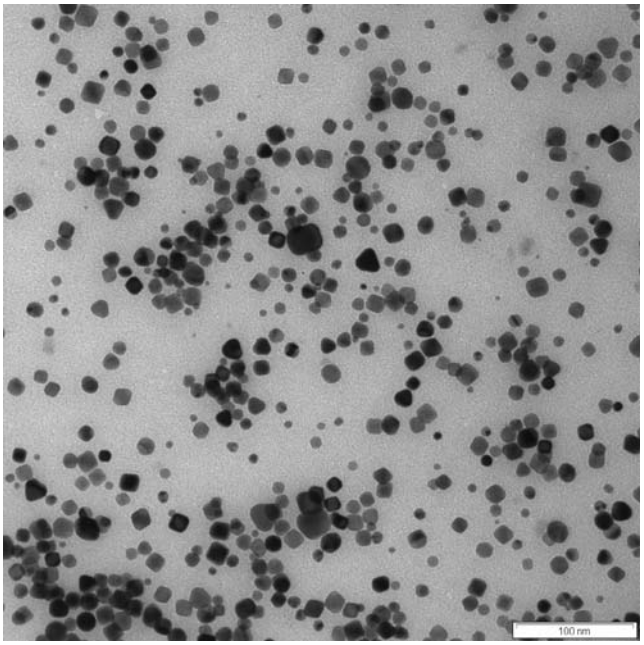

Fig. 6 TEM micrograph of gold nanoparticles prepared at 100 °C according to procedure C with sample VI

temperature. Therefore, an absorption maximum at 519 nm becomes detectable for sample V, in contrast to an absorption maximum at 420 nm for sample VII. In the other cases (sample III, IV, and VI) a plateau range between 430 and 560 nm was observed.

The mean particle size determined by dynamic light scattering measurements is varying between 1.5 and 3.5 nm (compare Table 2). Only in the case of the red colored Au solution prepared with sample V significant larger particle dimensions of about 9 nm were detected. Thus the heating procedure leads to quite similar results as received by procedure A at room temperature.

By using sample V the particle peak of the intensity plot at 9 nm coincides with the exclusive peak of the number plot indicating the formation of only one particle fraction. TEM micrographs indeed show 9-nm-sized spherical nanoparticles (compare Fig. 4).

The positive zeta potential values between +13 and +30 mV (compare Table 2) indicate that the gold nanoparticles are stabilized by the polyelectrolytes. However, due to the significant faster particle formation process at the elevated temperature the differences in the zeta potential between sample III and IV disappear, and electrostatically well-stabilized particles were obtained for the first time by using sample VII. This behavior can be explained by the better adsorption on the gold nanoparticles due to the disulfide head groups.

In general, structure type B and C can be successfully used for synthesizing gold nanoparticles also at higher temperature. Again, sample V with a higher content of dendritic units (structure type C) stabilizes larger gold nanoparticles (9 nm in size). Furthermore, sample VII exhibits the ability to stabilize significant smaller gold nanoparticles than the other samples with maltotriose units. However, the smallest particle dimensions were found in presence of sample III possessing the highest degree of linear units and the smaller maltose residue.

It has to be noted here that the nucleation process seems to be not influenced strongly by the faster process at 100 °C and therefore quite similar particle dimensions are observed in comparison to the very slow nucleation process at room temperature (compare data in Table 1).

Gold nanoparticle formation at 100 °C (procedure C, 3 min; weight ratio of PEI, metal=1:10)

When the mass ratio of Au to PEI is increased to 10:1, the solute concentration is increased drastically. The results, given in Table 3, show that the particle size can be increased drastically by this way. Already in the case of samples I and II a weak violet colored solution can be observed. In the case of sample V the particle growing process leads to significant larger particles which tend to sedimentate immediately.

In contrast to the previous experiments, red colored solutions with mean particle sizes between 9 and 15 nm for samples III, IV, VI, and VII (Table 3) are observed after

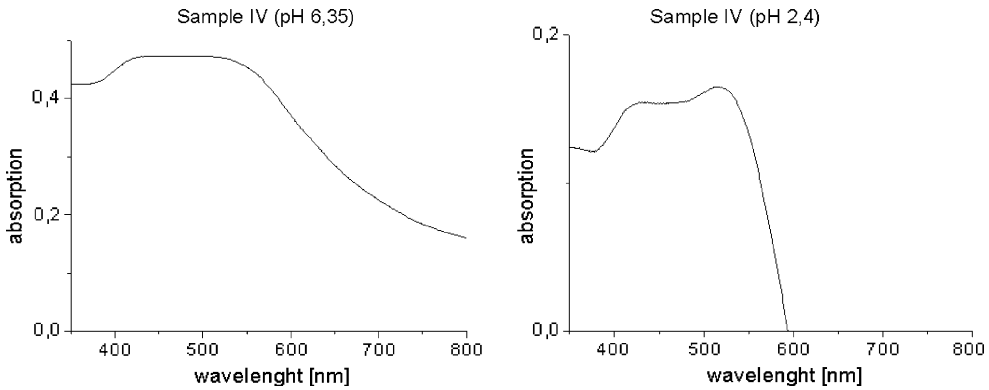

Fig. 7 UV-vis spectra of gold nanoparticles prepared at room temperature according to procedure A with sample IV at pH 6.35 and pH 2.4

cooling down to room temperature. Especially, the positive zeta potentials between +33 and +42 mV demonstrates electrostatically well-stabilized particles. For sample III with an absorption maximum at 561 nm, a mean particle size of 8.6 nm is determined by dynamic light scattering. The TEM micrographs show spherically sized nanoparticles of about 8 nm quite similar to that, demonstrated already in Fig. 4. However, again the smallest particle size is detected with sample III (structure type B) containing maltose units.

In presence of sample IV the mean particle size of the gold nanoparticles is increased to 15 nm. Therefore, spherically particles of the same dimensions can be visualized by TEM, but the size distribution becomes broader.

Sample VI and VII show a clear tendency to form triangular or cubic particles (10 nm in size) (Fig. 6).

Gold nanoparticle formation at room temperature by varying the pH

It has to be taken into account that a variation of the pH can induce quite different effects due to a change of the ionic strength, the basicity of the functional groups of the poly (ethyleneimine) as well as the coil dimensions of the PEI. The influence of the pH on the particle formation process was investigated in more detail at room temperature (procedure A) with sample IV. The UV-vis spectra show that the two absorption bands at 410 and 520 nm can be influenced by changing the pH (Fig. 7). As already mentioned before, at neutral pH conditions a plateau range is observed. At pH=2.4 the absorption band at 520 nm is increased, indicating the preferred formation of the larger particle fraction. In consequence the mean particle size determined by dynamic light scattering is shifted from 4.9 nm (at pH=6.35) to 7.1 nm (at pH=2.4). One can conclude that in the acidic pH range the reducing power of the secondary amino groups is enhanced due to the ion pair formation of the amino groups in the protonated state according to the mechanism discussed before, and schematized in Fig. 5. In consequence larger particles are formed.

Conclusions

Our experiments have shown differences in the reducing and stabilizing properties of the PEI samples in dependence on the degree of substitution with oligosaccharides. When mainly tertiary amino groups exist in the macromolecule (structure type A), a reduction of Au^{3+} to elementary gold is not possible. The presence of primary amino groups seems to be of importance with regard to the size and shape of the particles formed, but not yet of primary relevance with regard to the reducing power.

Therefore, the reduction process can be related to the amount of secondary amino groups, and a mechanism via an instable double bound between the secondary amino group and the methylene group in direct neighborhood can be discussed according to the mechanism already proposed by Wang et al. [41]. The much better reducing power at acidic pH range can be understood due to the favoured ion pair formation between the anionic $AuCl_4^-$ ions and the protonated amino groups in the first step of the interaction.

The smallest particle size is obtained in presence of sample III (structure type B) with an excess of linear units (secondary amino groups), which contains maltose units and a low molecular weight. In that case the electrostatic force in combination to the steric repulsion is strong enough to stabilize already very small gold nanoparticles or so called Au clusters of about 2 nm in size. That means already the primary formed nuclei are stabilized combined by simultaneous inhibition of the particle growth process by sample III. The quite outstanding properties of sample V can be related to the more dendritic structure with less L-units and maltotriose side groups. Here, uniform particles of larger dimensions are formed and stabilized.

An increase of the gold chloride concentration, and a shortening of the reaction time leads to the formation of significant larger gold particles. In general, the nanoparticles formed are stable for a long time (up to now more than 8 months).

Finally, one can conclude that (a) tertiary amino groups are inactive in the reduction process, (b) secondary amino groups are the major reducing components, (c) primary amino groups have a stabilizing effect and influence the particle shape, and (d) oligosaccharide groups offer a strong steric stabilizing effect allowing for the formation of very small gold particles. In addition they can influence the particle size and shape.

Thus, the final particle size and shape can be tuned by changing the solute concentration, the time of heating, and the pH value. However, the oligosaccharide-modified poly (ethyleneimines) used here does not even lead to monodisperse particles. Therefore we plan to synthesize more suited oligosaccharide-modified PEI samples in the future.

References

1. Willner I, Katz E (2004) Angew Chem 116:6166
2. Huang XH, Jain PK, El-Sayed HI, El-Sayed MH (2007) Nanomedicine 2:681
3. Daniel MC, Astruc D (2004) Chem Rev 104:293
4. Hayat MA (1989) Colloidal Gold: Principles, Methods, and Applications. Academic, New York
5. Gupta S, Huda S, Kilpatrick PK, Velev OD (2007) Analytical Chem 79:3810
6. Li HX, Nelson E, Pentland A, van Buskirk J, Rohberg L (2007) Plasmonics 2:165

7. Kolosova AY, De Saeger S, Sibanda L, Verheijen R, van Peteghem C (2007) Anal Bioanal Chem 389:2103
8. Texter J (2001) Reactions and Synthesis in Surfactant Systems Surfactant Science Series 100. Marcel Dekker, New York
9. Jena BK, Raj CR (2007) J Phys Chem C 111:15146
10. Mokhonoana M, Coville NJ, Datye A (2004) Stud Surf Sci Catal A 154:827
11. Turkevich J, Stevenson PC, Hiller J (1951) Discuss Faraday Soc 11:55
12. Koetz J, Kosmella S (2007) Polyelectrolytes and Nanoparticles. Springer, Berlin Heidelberg
13. Bertino MF, Sun ZM, Zhang R, Wang LS (2006) J Phys Chem B 110:21417
14. Yang Y, Chen S (2003) Nano Lett 3:75
15. Mayer ABR, Mark JE (1998) Eur Polym J 34:103
16. Kim F, Connor S, Song H, Kuykendall T, Yang P (2004) Angew Chem Int Ed 43:3673
17. Filali M, Meier MAR, Schubert US, Gohy JF (2005) Langmuir 21:7995
18. Mayer ABR, Mark JE (2000) Polymer 41:1627
19. Mayer ABR, Mark JE (1997) Colloid Polym Sci 275:333
20. Corbierre MK, Cameron NS, Lennox RB (2004) Langmuir 20:2867
21. Ulrich S, Laguecir A, Stoll S (2005) Macromolecules 38:8939
22. Mayya KS, Schoeler B, Caruso F (2003) Adv Funct Mater 13:183
23. Schuetz P, Caruso F (2004) Chem Mater 16:3066
24. Pugh TL, Heller W (1960) Polym Science 47:219
25. Chen CC, Hsu CH, Kuo PL (2007) Langmuir 23:6801
26. Sharma G, Ballauff M (2004) Macromol Rapid Commun 25:547
27. Sun X, Dong S, Wang E (2005) J Colloid Interface Sci 205:301
28. Sun X, Dong S, Wang E (2004) Polymer 45:2181
29. Note C, Kosmella S, Koetz J (2006) Colloids Surf A: Pysicochem Eng Asp 290:150
30. Sun X, Zhang ZL, Wang E (2003) Chinese Chem Lett 14:866
31. Esumi K, Hosoya T, Suzuki A, Torigoe K (2000) Langmuir 16:2978
32. Pérignon N, Marty JD, Mingotaud AF, Dumont M, Rico-Lattes I, Mingotaud C (2007) Macromolecules 40:3034
33. Krämer M, Pérignon N, Haag R, Marty JD, Thomann R, Lauth-de Viguerie N, Mingotaud C (2005) Macromolecules 38:8308
34. Fuente JM, Barrientos AG, Rojas TC, Rojo J, Canada J, Fernandez A, Penades S (2001) Angew Chem Int Ed 40(12):2257
35. Housni A, Cai H, Liu S, Pun SH, Narain R (2007) Langmuir 23:5056
36. Halkes KM, Carvalho de Souza A, Maljaars P, Gerwig GJ, Kamerling JP (2005) Eur J Org Chem 3650
37. Cai QY, Kim SH, Choi KS, Kim SY, Byun SJ, Kim KW, Park SH, Juhng SK, Yoon KH (2007) Investigative Radiology 42:797
38. Appelhans D, Zhong Y, Komber H, Friedel P, Oertel U, Scheler U, Morgner N, Kuckling D, Richter S, Brutschy B, Voit B (2007) Macromol Biosci 7:373
39. Klajnert B, Appelhans D, Komber H, Morgner N, Schwarz S, Richter S, Brutschy B, Ionov M, Tonkikh A K, Bryszewska M, Voit B (2008) Chem Eur J doi:10.1002/chem200800342
40. Kaszuba M, McKnight D, Connah MT, McNeil-Watson FK, Nobbmann U (2008) J Nanopart Res 10:823
41. Wang ST, Yan JC, Chen L (2005) Mater Lett 59:1383
42. Kelly KL, Coronado E, Zhao LL, Schatz GC (2003) J Phys Chem B 107:668
43. Mirkin CA, Letsinger RL, Mucic RC, Storhoff JJ (1996) Nature 382:607
44. Witten KG, Bretschneider JC, Eckert T, Richtering W, Simon U (2008) Phys Chem Chem Phys 10:1870
45. Park SY, Lee J-S, Georganopoulu D, Mirkin CA, Schatz GC (2006) J Phys Chem B 110:12673
46. Niemeyer CM, Simon U (2005) Eur J Inorg Chem 3641
47. Nykypanchuk D, Maye MM, Van der Lelie D, Gang O (2008) Nature 451:549
48. Lo CK, Paau MC, Xiao D, Choi MMF (2008) Anal Chem 80:2439
49. Wen F, Englert U, Gutrath B, Simon U (2008) Eur J Inorg Chem 106